ORIGINAL ARTICLE

Usman Allauddin · **Sai Ranjith Reddy Lomada** ·
Michael Pfitzner

Investigation of pressure and the Lewis number effects in the context of algebraic flame surface density closure for LES of premixed turbulent combustion

Abstract Large scale industrial combustion devices, for example, internal combustion engines, gas turbine combustors, etc., operate under high-pressure conditions and utilize a variety of fuels. Unfortunately, the majority of the current numerical combustion modelling approaches are not fully validated for high-pressure and the non-unity Lewis number (Le = thermal diffusivity/mass diffusivity) effects in premixed turbulent combustion. In any case, a numerical model needs to be checked for the effects of these parameters to guarantee generality of the model. In the present study, these two critical features of the models are numerically explored utilizing fundamental elements of several algebraic flame surface density reaction rate closure models accessible in the open literature. The Lewis number impact is likewise examined utilizing LES of recently published subgrid scale fractal flame surface density model, which indicated acceptable results for high and low-pressure methane fuelled applications. The computed numerical results are compared with an extensive experimental dataset for lean methane and propane fuels featuring various flow and turbulence conditions at operating pressures in the range of 1–10 bar. The quantitative results from most of the selected models do not show the experimentally observed trends at high-pressures and for non-unity Le number fuels. Modifications to the models are incorporated to reflect effects of these two important parameters utilizing a broad parametric investigation resulting in a satisfactory agreement with the experimental data.

List of symbols

c	Reaction progress variable
C_A	Angelberger model constant
C_D	Keppeler model constant
C_K	Keppeler model constant
C_Z	Zimont model constant
D	Fractal dimension
Da	Damköhler number

U. Allauddin · S. R. R. Lomada · M. Pfitzner
Institut für Thermodynamik, Fakultät für Luft-und Raumfahrttechnik, Universität der Bundeswehr München, 85579 Neubiberg, Germany

U. Allauddin (✉)
Department of Mechanical Engineering, NED University of Engineering and Technology, Karachi 75270, Pakistan
E-mail: usman.allauddin@neduet.edu.pk

k	Turbulent kinetic energy (m^2/s^2)
Ka_Δ	Subgrid Karlovitz number
l	Integral length scale of turbulence (m)
Le	Lewis number
Ma	Markstein number
p	Pressure, Pa
Re	Reynolds number
s_T	Turbulent flame speed (m/s)
s_L^0	Un-stretched laminar flame speed (m/s)
s_L	Stretched laminar flame speed (m/s)
S_{ij}	Shear stress tensor (1/s)
Sc_t	Schmidt number
t	Time (s)
T	Temperature (K)
$u^{'}$	RMS turbulent velocity (m/s)
$u^{'}_\Delta$	Subgrid scale velocity fluctuations (m/s)
u_i	Velocity component (m/s)
U	Bulk velocity at inlet (m/s)
x_i	Spatial coordinate i (m)

Greek letters

α	Diffusivity (m^2/s)
α_{th}	Thermal diffusivity (m^2/s)
Γ	Efficiency function
l_F	Laminar flame thickness (m)
Δ	Filter size (m)
ε_i	Inner cut off scale (m)
ε_o	Outer cut off scale (m)
κ	Flame stretch rate (1/s)
κ_s	Flame strain rate (1/s)
μ	Dynamic viscosity (kg/ms)
ν	Kinematic viscosity (m^2/s)
ρ	Density (kg/m^3)
Σ_{gen}	Flame surface density (1/m)
τ	Heat release factor
φ	Flame angle, radian
$\dot{\omega}$	Turbulent reaction source term (kg/m^3s)
$\varXi$	Flame wrinkling factor

Superscripts and subscripts

b	Burned state
i	Inner
o	Outer
res	Resolved
sgs	Subgrid scale
t	Turbulent
u	Unburned state

Abbreviations

AFSD	Algebraic flame surface density
DNS	Direct numerical simulation

FSD   Flame surface density
LES   Large Eddy simulation
RANS   Reynolds-averaged Navier Stokes
RHS   Right-hand-side of an equation
SGSF   Subgrid scalar flux

1 Introduction

Large Eddy Simulation (LES) has shown potential to improve upon conventional Reynolds-averaged Navier Stokes (RANS) simulations for the predictions of turbulent reactive flows. However, the turbulent premixed combustion modelling faces the problem that the flame thickness is smaller than the typical LES filter sizes. Thus, a model is required to describe the extent of subgrid scale flame wrinkling. A few modelling approaches have been proposed by various scientists to overcome this issue, for example, the flame front tracking strategy (level-set of G-equation) [1,2], the Artificially Thickened Flame (ATF) procedure [3,4] and the idea of Flame Surface Density (FSD) [5,6]. The well-established FSD based reaction rate closure approach exists with two principle variations. In one methodology, the closure is achieved through mathematical expressions [5], while the other one includes solving an additional FSD transport equation [6]. Various Algebraic Flame Surface Density (AFSD) models have been created and applied for premixed flame burners [7,8]. They can be simpler, less expensive in terms of computational time and numerically more robust than models featuring a FSD transport equation, which however might be able to incorporate some non-equilibrium effects between production and destruction of FSD. The AFSD models are the focal point of the present work. Many practical industrial devices using premixed combustion operate under high-pressure conditions with a variety of fuels. So, a numerical model should account for the influence of pressure p and fuel effects on reaction closure to claim any generality. However, the greater part of the current AFSD models have been validated just for atmospheric methane flames and frequently using relatively fine LES computational grids, where the subgrid wrinkling factor $\varXi$ approaches one.

Pressure is known to influence both the turbulent flow field through variation of viscosity and laminar premixed flame structure by decreasing the flame thickness and flame speed. It has been observed experimentally by different researchers [9–11] that the flame wrinkling increases, the smaller turbulence scales (Taylor scales, Kolmogorov scales) shrink while the turbulent integral length scale remains nearly unchanged with increase of pressure if inlet velocity is left constant. The kinematic viscosity ν = absolute viscosity/density = μ/ρ is proportional to $1/p$, so increased pressure results in higher turbulent Reynolds number $\mathrm{Re_t} = u' l/\nu$, if the mean bulk velocity is kept constant, typically the turbulence intensity is also weakly influenced by pressure. Here l and u' refer to integral length scale and root mean square (RMS) turbulent velocity. The smallest turbulence scales shrink with increasing $\mathrm{Re_t}$, so estimated turbulence energy spectra are moved to higher wavenumbers [9]. The un-stretched laminar flame speed s_L^0 and Zeldovich flame thickness l_F also vary with pressure. The pressure scaling for methane and propane air mixtures are $s_\mathrm{L}^0 \propto p^{-0.5}, l_F \propto p^{-0.5}$ and $s_\mathrm{L}^0 \propto p^{-0.26}, l_F \propto p^{-0.74}$, respectively [1,12,13].

Experimental investigation of turbulent reacting flows under high-pressure conditions is very difficult and costly. With the recent advances in computational technology and availability of super powered computational clusters, Direct Numerical Simulation (DNS) is increasingly used to study turbulent reacting flows under high-pressure conditions [14–18]. These DNS based studies help the development and validation of numerical models applicable to conditions typical in the industry devices. The complexity of the high-pressure combustion puts tough requirements on the numerical models. Only a few numerical models in the open literature, mainly in the RANS context, are dealing specifically with the pressure dependence of turbulent premixed combustion [19]. Authors Dinkelacker, Muppala, Aluri et al. have contributed to turbulent premixed combustion modelling at high-pressures [20–24]. Muppala et al. [20] developed an algebraic turbulent premixed combustion model to correctly predict the turbulent flame speed s_T for different fuels under high-pressure conditions in the RANS context. The model showed satisfactory performance for methane, propane and ethylene fuels for pressures up to 10 bar. An explicit pressure correction term $(p/p_0)^n$, where p_0 = atmospheric pressure = 1 bar, p is the operating pressure in bar and exponent n is a constant, was incorporated in the algebraic wrinkling factor expression to correctly predict the experimentally observed pressure dependency of turbulent flame speeds. Aluri et al. [21] investigated the performance of two algebraic flame surface density models including the FSD model of Muppala et al. [20] for high-pressure methane flames. They found a very good performance of the models (with explicit pressure correction term) for different turbulence conditions under high-pressures.

Aluri et al. [22] also investigated the performance of Lindstedt and Váos model [25] with explicit pressure and Lewis number correction terms. They reported very good performance of the tuned model in terms of showing the effects of high-pressure and non-unity Le number fuels on the reaction source term. Keppeler et al. [26] presented a FSD premixed combustion model based on the fractal approach in the LES context. The model showed excellent performance for high-pressure flames at conditions typical for spark ignition engines, gas turbines, etc. Allauddin et al. [27] investigated the performance of a simplified version of the model presented by Keppeler et al. [26]. The simplifications to the original model were discussed and the performance of the new model was compared with the original model and experimental data. The original and simplified models were found suitable for predicting the performance of turbulent premixed flames under high-pressure conditions. Recently, Allauddin et al. [28] extended the Keppeler model [26] to the RANS context. The performance of the new RANS model was compared with the original LES model and experimental data. The RANS model showed similarly satisfactory performance in terms of predicting the turbulent flame speeds and flame structures of turbulent premixed flames at high-pressure conditions.

The influence of Le number on the turbulent reaction rate is explained elaborately in the work of Lipatnikov and Chomiak [29]. Le >1 represents a faster heat diffusion compared to diffusion of species, which may result in reduced turbulent flame propagation. So, the numerical models without explicit Le number dependency might predict higher values of turbulent flame speed especially at moderate to high turbulence. High Le number fuels have applications in spark ignition engines, gas turbines, etc., therefore, examination of the fuel effects on flame characteristics at high-pressures is crucial. Le number effects in highly turbulent premixed flames have been investigated in [30] and particularly for high-pressure conditions in [11]. In the RANS context, a 1/Le dependence of the algebraic FSD reaction rate closure was discovered effective for Le $\geq$ 1 fuels for pressures up to 10 bar [26]. The model was also extended to the LES context and checked for its relevance for a Bunsen-like burner, a sudden expansion dump combustor and a typical swirl-stabilised gas turbine combustor [8] indicating good agreement with the experiments. In [24], the RANS model is utilized to simulate lean premixed turbulent methane/hydrogen/air flames (Le $\leq$ 1). The reaction rate closure approach with 1/Le prefactor was found to give a generally good agreement for all the flames with hydrogen content up to 20% and a reasonable agreement for 30% and 40% hydrogen. Chakraborty and Cant [31] also reported that the estimate $\overline{(\rho S_d)}_S \approx \rho_u s_L$ is not valid for non-unity Le number fuels and recommended

$$\overline{(\rho S_d)}_S \approx \rho_u s_L/\mathrm{Le},\tag{1}$$

where ρ, ρ_u, S_d and s_L represent the density, density of unburnt reactants, flame displacement speed and stretched laminar flame speed, respectively, while the subscript S outside the parenthesis on left hand side of Eq. (1) refers to the surface filtering. In a recent study [32], based on a-priori analysis of DNS data for a range of different Le numbers, the performance of several subgrid scalar flux (SGSF) models and algebraic FSD models in the context of turbulent premixed combustion is investigated on an individual basis and in terms of their combined interactions. It is reported that the Le number correction given by Eq. (1) essentially improves the prediction of the surface-weighted filtered values of density-weighted displacement speed. The Le number expression (1/Le) is utilized in the present investigation to incorporate the fuel effects.

The focal point of the present study is to investigate some of the well-known AFSD models under high-pressure and non-unity Le number conditions. The chosen models are proposed by Angelberger et al. [33], Fureby [34] and Zimont [35]. The central elements of these models as utilized in the LES simulations are presented in Table 1. The resulting models are named Model-A, Model-F and Model-Z in the rest of the paper. An already developed LES subgrid combustion model [26], which indicated a good performance for turbulent Bunsen flames over a wide range of turbulence and pressures in the range of 1–20 bar, is additionally investigated for non-unity Le number fuel. This model is referred to Model-K in the rest of the paper.

In the current work, the Model-K is adapted only for Le variation as its performance for high-pressure conditions is already investigated in the previous study [26]. The model-F is found to be extensively used by different researchers in the open literature. Therefore, the performance of this model is investigated for both high-pressure conditions and non-unity Le number fuel (Sect. 6.3). The expression 1/Le used in the Model-K is also used in the Model-F to bring the Le number dependency in the model. The results show that the adapted Model-K and Model-F give a quite good performance for non-unity Le number fuels and a reasonable agreement with the experiments. For the sake of brevity, the Model-A and Model-Z are only adapted for pressure variation. The authors expect that 1/Le prefactor would have a similar effect in these models to correctly repesent the Le number dependency of turbulent flame speed. The numerical predictions from the current study are compared with the experimental data of Kobayashi et al. [9,12,36].

Table 1 The main expressions of the AFSD models used in the current study

Model title	Original form	Adapted form
Model-A	$\Gamma = A * exp\left[\dfrac{-B}{\left(u'_\Delta/s_L\right)^{0.3}}\right] * \left(\dfrac{\Delta}{l_F}\right)^{2/3}$	$\Gamma = A * exp\left[\dfrac{-B}{\left(u'_\Delta/s_L\right)^{0.3}}\right] * \left(\dfrac{\Delta}{l_F}\right)^{2/3}$
	$A = 0.75, B = 1.2$	$A = 9.5, B = 1.2$
	$\Xi = \left[1 + C_A \Gamma \dfrac{u'_\Delta}{s_L}\right]$	$\Xi = \left[1 + C_A C_p \Gamma \dfrac{u'_\Delta}{s_L}\right]$
	$C_A = 1.0$	$C_A = 0.4, C_p = \left(\dfrac{p}{p_o}\right)^n, n = -0.25$
Model-F	$\Gamma = A * exp\left[\dfrac{-B}{\left(u'_\Delta/s_L\right)^{0.3}}\right] * \left(\dfrac{\Delta}{l_F}\right)^{2/3}$	$\Gamma = A * exp\left[\dfrac{-B}{\left(u'_\Delta/s_L\right)^{0.3}}\right] * \left(\dfrac{\Delta}{l_F}\right)^{2/3}$
	$A = 0.75, B = 1.2$	$A = 9.5 B = 1.2$
	$\varepsilon_i = \dfrac{s_L \Delta}{u'_\Delta \Gamma}, \varepsilon_o = \Delta$	$\varepsilon_i = \max\left(\dfrac{s_L \Delta}{u'_\Delta \Gamma}, l_F\right), \varepsilon_o = \Delta$
	$D = \dfrac{2.05 s_L}{u'_\Delta + s_L} + \dfrac{2.35 u'_\Delta}{u'_\Delta + s_L}$	$D = \dfrac{8/3 \mathrm{Ka}_\Delta + 2 C_D}{\mathrm{Ka}_\Delta + C_D}, C_D = 0.03$
	$\Xi = \left(\dfrac{\varepsilon_o}{\varepsilon_i}\right)^{D-2}$	$\Xi = C_{Le}\left(1 + \dfrac{\varepsilon_o}{\varepsilon_i}\right)^{D-2}, C_{Le} = 1/\mathrm{Le}$
Model-K	$\varepsilon_i = \max\left(l_F \mathrm{Ka}_\Delta^{-1/2}, 2l_F\right)$	$\varepsilon_i = \max\left(l_F \mathrm{Ka}_\Delta^{-1/2}, 2l_F\right)$
	$\varepsilon_o = 2.2\Delta$	$\varepsilon_o = 2.2\Delta$
	$D = \dfrac{8/3 \mathrm{Ka}_\Delta + 2 C_D}{\mathrm{Ka}_\Delta + C_p}, C_D = 0.03$	$D = \dfrac{8/3 \mathrm{Ka}_\Delta + 2 C_D}{\mathrm{Ka}_\Delta + C_p}, C_D = 0.03$
	$\mathrm{Ka}_\Delta = \left(\dfrac{u'_\Delta}{s_L^0}\right)^{\frac{3}{2}} \left(\dfrac{\Delta}{l_F}\right)^{-\frac{1}{2}}$	$\mathrm{Ka}_\Delta = \left(\dfrac{u'_\Delta}{s_L^0}\right)^{\frac{3}{2}} \left(\dfrac{\Delta}{l_F}\right)^{-\frac{1}{2}}$
	$\Sigma_{gen} = C_K \left(\dfrac{\varepsilon_o}{\varepsilon_i}\right)^{D-2} \tilde{c}(1-\tilde{c})|\nabla \tilde{c}| F(\tilde{c})^{-1}$	$\Sigma_{gen} = C_K C_{Le} \left(\dfrac{\varepsilon_o}{\varepsilon_i}\right)^{D-2} \tilde{c}(1-\tilde{c})|\nabla \tilde{c}| F(\tilde{c})^{-1}$
	$C_K = 4.5$	$C_K = 4.5, C_{Le} = 1/\mathrm{Le}$
	$\Xi = \left(\dfrac{\varepsilon_o}{\varepsilon_i}\right)^{D-2}$	$\Xi = \left(\dfrac{\varepsilon_o}{\varepsilon_i}\right)^{D-2}$
Mode-Z	$\Xi = \left[1 + C_Z \left(\dfrac{u'_\Delta}{s_L}\right)^{3/4} \left(\dfrac{\Delta}{l_F}\right)^{1/4}\right]$	$\Xi = \left[1 + C_Z C_p \left(\dfrac{u'_\Delta}{s_L}\right)^{3/4} \left(\dfrac{\Delta}{l_F}\right)^{1/4}\right]$
	$C_Z = 0.51$	$C_Z = 1.2, C_p = \left(\dfrac{p}{p_o}\right)^n, n = 0.15$

The paper is organized as follows. First, a short description of the chosen AFSD models is presented. Second, the sections describing the experimental data utilized for the validation of the computed results and numerical setup are presented. Results are discussed in Sect. 6. The conclusions of the work are presented in the last section.

2 Mathematical background and description of numerical models

The reaction progress variable c for turbulent premixed combustion at constant pressure can be expressed in terms of temperature T as $c = (T - T_u)/(T_b - T_u)$ which changes monotonically from 0 in reactants to 1 in totally burned products. Here subscripts u and b indicate unburnt and burnt states, respectively. Following [13] and assuming unity Le number, adiabaticity and low Mach number, the Favre-filtered transport equation for c becomes

$$\frac{\partial \bar{\rho}\tilde{c}}{\partial t} + \frac{\partial \bar{\rho}\tilde{c}\tilde{u}_i}{\partial x_i} + \frac{\partial}{\partial x_i}\left(\overline{\bar{\rho}u_i c} - \bar{\rho}\tilde{u}_i \tilde{c}\right) = \frac{\partial}{\partial x_i}\left(\overline{\rho\alpha \frac{\partial c}{\partial x_i}}\right) + \bar{\dot{\omega}}, \tag{2}$$

where u_i, α, $\dot{\omega}$ represent the ith component of flow velocity vector, progress variable diffusivity, progress variable chemical reaction rate, respectively. The overbar indicates a LES filtering operation and tilde represents Favre filtering. Utilizing the FSD method, the sum of the molecular diffusion of the reaction progress variable and the LES filtered reaction rate can be written as

$$\frac{\partial}{\partial x_i}\left(\overline{\rho\alpha \frac{\partial c}{\partial x_i}}\right) + \bar{\dot{\omega}} = \overline{\rho S_d |\nabla c|} \approx \rho_u s_L \Sigma_{gen}, \tag{3}$$

where $\Sigma_{\text{gen}} = |\overline{\nabla c}|$ is the total subgrid FSD and the surface-filtered value of the density weighted displacement speed $\overline{(\rho S_d)}_S$ is approximated as $\rho_u s_L$. The FSD can be expressed in terms of the subgrid scale wrinkling factor $\Xi = |\overline{\nabla c}|/|\nabla \bar{c}|$ yielding

$$\frac{\partial}{\partial x_i} \left(\overline{\rho \alpha \frac{\partial c}{\partial x_i}} \right) + \bar{\dot{\omega}} = \rho_u s_L \Sigma_{\text{gen}} = \rho_u s_L \Xi \, |\nabla \bar{c}|. \tag{4}$$

The fractal characteristic of premixed flames is notable and has been well demonstrated experimentally. The wrinkling factor Ξ can be expressed in the form proposed by Gouldin [37]

$$\Xi = \left(\frac{\varepsilon_o}{\varepsilon_i} \right)^{D-2}, \tag{5}$$

where ε_i, ε_o and D indicate inner and outer cut-off scales and a fractal dimension, respectively. Fractal based models obviously need accurate models for the fractal dimension and cut-off scales.

The other term, which should be modelled in Eq. (2), is the subgrid scalar transport $(\bar{\rho}\widetilde{u_i c} - \bar{\rho}\tilde{u}_i \tilde{c})$ In the current work, it is modelled utilizing the gradient hypothesis

$$\bar{\rho}\widetilde{u_i c} - \bar{\rho}\widetilde{u}_i \tilde{c} = -\frac{\mu_{\text{sgs}}}{Sc_t} \frac{\partial \tilde{c}}{\partial x_i}, \tag{6}$$

where Sc_t and μ_{sgs} indicate the turbulent Schmidt number and subgrid scale dynamic viscosity. When utilizing the gradient hypothesis based model, counter gradient subgrid scalar fluxes are ignored. According to Boger et al. [5] in LES the unresolved contribution of the turbulent fluxes is considered to be small; the major contributions of the gradient and counter gradient scalar fluxes are expected to be captured at the resolved scales. Also, the use of $|\overline{\nabla c}|$ rather than $|\nabla \bar{c}|$ in the LES expression of Σ_{gen} (as used in the present investigation) comprises a certain implicit counter gradient subgrid scalar flux model as reported in the work of Klein *et al.* [32] and Allauddin *et al.* [38]. In the LES, we solve the following transport equation for the Favre filtered reaction progress variable $\tilde{c}$

$$\frac{\partial \bar{\rho}\tilde{c}}{\partial t} + \frac{\partial \bar{\rho}\tilde{c}\tilde{u}_i}{\partial x_i} = \rho_u s_L \Xi \, |\nabla \tilde{c}| + \frac{\partial}{\partial x_i} \left(\frac{\mu_{\text{sgs}}}{Sc_t} \frac{\partial \tilde{c}}{\partial x_i} \right). \tag{7a}$$

Comparison to Eq. (4) shows explicitly the implicit counter-gradient model (last term on RHS)

$$\frac{\partial \bar{\rho}\tilde{c}}{\partial t} + \frac{\partial \bar{\rho}\tilde{c}\tilde{u}_i}{\partial x_i} = \rho_u s_L \Xi \, |\nabla \bar{c}| + \frac{\partial}{\partial x_i} \left(\frac{\mu_{\text{sgs}}}{Sc_t} \frac{\partial \tilde{c}}{\partial x_i} \right) - \rho_u s_L \Xi \left(|\nabla \tilde{c}| - |\nabla \bar{c}| \right). \tag{7b}$$

Recent studies [32,38] show that LES results obtained with the FSD model using $|\nabla \tilde{c}|$ in the reaction rate modelling will not improve when more advanced subgrid scalar flux closures explicitly representing the effect of counter-gradient diffusion are used.

The subgrid scale velocity fluctuations u'_Δ are determined as $u'_\Delta = \sqrt{2k_{\text{sgs}}/3}$. The subgrid turbulent kinetic energy k_{sgs} and subgrid scale viscosity are determined by utilizing the one equation eddy viscosity model proposed by Schumann [39] and further improved by Fureby et al. [40] with a transport equation for k_{sgs}

$$\frac{\partial \bar{\rho}k_{\text{sgs}}}{\partial t} + \frac{\partial \left(\bar{\rho}\tilde{u}_i k_{\text{sgs}} \right)}{\partial x_i} - \frac{\partial}{\partial x_i} \left(\mu_{eff} \frac{\partial k_{\text{sgs}}}{\partial x_i} \right) = -\bar{\rho} S_{ij} B_{ij} - C_e \bar{\rho} \frac{k_{\text{sgs}}^{\frac{3}{2}}}{\Delta}, \tag{8}$$

$$B_{ij} = \frac{2}{3} k_{\text{sgs}} \delta_{ij} - 2\nu_\Delta \left\{ S_{ij} - \frac{1}{3}\text{tr} \left(S_{ij} \right) \delta_{ij} \right\}, \mu_{\text{sgs}} = C_K \bar{\rho}\sqrt{k_{\text{sgs}}}\Delta, \nu_\Delta = C_K \sqrt{k_{\text{sgs}}}\Delta, \tag{9}$$

where $S_{ij} = 0.5 \left(\partial \tilde{u}_i / \partial x_j + \partial \tilde{u}_j / \partial x_i \right)$ is the resolved strain rate, $\mu_{eff} = \mu + \mu_{\text{sgs}}$ is the effective viscosity with ν_Δ being eddy kinematic subgrid viscosity and Δ is the filter size. In the present study, the model coefficients C_e and C_K are taken as 1.05 and 0.095, respectively. Model-A and Model-F additionally require

Table 2 The un-stretched laminar flame speed, Zeldovich flame thickness and Markstein number values used in the current study

Pressure (bar)	Methane			Propane		
	s_L^0 (m/s)	$l_F * 10^{-4}$ (m)	Ma	s_L^0 (m/s)	$l_F * 10^{-4}$ (m)	Ma
1	0.345	0.456	0.82	0.42	0.620	5.6
5	0.155	0.210	0.55	0.23	0.136	2.0
10	0.110	0.143	0.47	–	–	–

the estimation of an efficiency function, which represents the net straining effect of all the vortices smaller than the LES filter width Δ. The efficiency function Γ utilized in Model-A and Model-F is modelled as

$$\Gamma = A*exp\left[\frac{-B}{(u'_\Delta/s_L)^{0.3}}\right]*\left(\frac{\Delta}{l_F}\right)^{2/3},$$ (10)

where $A = 0.75$ and $B = 1.2$.

The stretched laminar flame speed s_L is modelled using the linear theory of instabilities [41]

$$s_L = s_L^0 - \text{Ma}\,\kappa l_F,$$ (11)

where s_L^0 and Ma represent the un-stretched laminar flame speed and Markstein number, respectively. The experimental values of these parameters [12,42] are used in the current study and are summarized in Table 2. The effective stretch κ is determined considering just strain effects, modelled by Hawkes and Cant [43]

$$\kappa \approx \kappa_s = (\delta_{ij} - n_{ij})\frac{\partial \tilde{u}_i}{\partial x_i} + \Gamma_s\frac{\sqrt{k_{sgs}}}{\Delta},$$ (12a)

utilizing a second efficiency function Γ_s as proposed by [44]. Here δ_{ij} is the Kronecker delta, $n_{ij} = (\bar{N}_i)_s(\bar{N}_i)_s + (\delta_{ij}/3)[1 - (\bar{N}_K)_s(\bar{N}_K)_s]$ is the flame orientation factor with $(\bar{N}_i)_s = -(\partial\bar{c}/\partial x_i)/\Sigma_{gen}$ being the ith component of flame surface-weighted normal vector. The first and second terms in the RHS of Eq. (12a) represent strain rates resulting from resolved and unresolved scales, respectively. The second efficiency function Γ_s is determined as

$$\log_{10}(\Gamma_s) = \frac{-1}{s+0.4}\exp\{-(s+0.4)\} + [1 - \exp\{-(s+0.4)\}]\left\{\sigma\left(\frac{u'_\Delta}{s_L^0}\right)s - 0.11\right\},$$ (12b)

$$s = \log_{10}\left(\frac{\Delta}{l_F}\right), \sigma\left(\frac{u'_\Delta}{s_L^0}\right) = \frac{2}{3}\left[1 - 0.5exp\left\{-\left(\frac{u'_\Delta}{s_L^0}\right)^{1/3}\right\}\right], u'_\Delta = \left(\frac{2}{3}k_{sgs}\right)^{0.5}.$$ (12c)

In the following subsections a short description of the FSD models used in the present study will be presented for completeness.

2.1 Brief description of Model-A and Model-F

Angelberger et al. [33] based their model on DNS data of flame stretch and vortex pair interaction [41] and expressed Ξ as

$$\Xi = \left[1 + C_A\Gamma\frac{u'_\Delta}{s_L}\right],$$ (13)

where $C_A = 1$ is a model constant.

Fureby [34] built his model on a fractal approach of Ξ, which is given by Eq. (5). In this model the inner and outer cut-off scales, fractal dimension and wrinkling factor are given by

$$\varepsilon_i = \frac{s_L\Delta}{u'_\Delta\Gamma},$$ (14a)

$$\varepsilon_{\mathrm{o}} = \Delta, \tag{14b}$$

$$D = \frac{2.05 s_{\mathrm{L}}}{u'_{\Delta} + s_{\mathrm{L}}} + \frac{2.35 u'_{\Delta}}{u'_{\Delta} + s_{\mathrm{L}}}, \tag{14c}$$

$$\varXi = \left(\frac{\varepsilon_{\mathrm{o}}}{\varepsilon_{\mathrm{i}}}\right)^{D-2}. \tag{14d}$$

2.2 Brief description of Model-K

Keppeler et al. [26] also used the fractal approach, using ideas from the RANS model of Lindstedt and Váos [25] in his extension to LES. In this model the inner and outer cut-off scales, fractal dimension, generalised FSD and wrinkling factor terms are defined as

$$\varepsilon_{\mathrm{i}} = \max\left(l_F \mathrm{Ka}_{\Delta}^{-1/2}, 2l_F\right), \tag{15a}$$

$$\varepsilon_{\mathrm{o}} = 2.2\Delta, \tag{15b}$$

$$D = \frac{8/3\mathrm{Ka}_{\Delta} + 2C_{\mathrm{D}}}{\mathrm{Ka}_{\Delta} + C_{\mathrm{D}}}, \ \mathrm{Ka}_{\Delta} = \left(\frac{u'_{\Delta}}{s_{\mathrm{L}}^0}\right)^{\frac{3}{2}} \left(\frac{\Delta}{l_F}\right)^{-\frac{1}{2}}, \tag{15c}$$

$$\Sigma_{\mathrm{gen}} = C_{\mathrm{K}} \left(\frac{\varepsilon_{\mathrm{o}}}{\varepsilon_{\mathrm{i}}}\right)^{D-2} \tilde{c}\,(1 - \tilde{c})\,|\nabla\tilde{c}|\,F\,(\tilde{c})^{-1}, \tag{15d}$$

$$\varXi = \left(\frac{\varepsilon_{\mathrm{o}}}{\varepsilon_{\mathrm{i}}}\right)^{D-2}, \tag{15e}$$

where $C_{\mathrm{K}} = 4.5$ and $C_{\mathrm{D}} = 0.03$ are model constants while Ka_{Δ} represents the subgrid Karlovitz number. In the CFD implementation, $F\,(\tilde{c})$ is approximated by a simple polynomial fit: $F\,(\tilde{c}) = a_1 - a_2\,(\tilde{c} - 0.5)^2 - a_3\,(\tilde{c} - 0.5)^4$ with $a_1 = 1.00, a_2 = 2.82$ and $a_3 = 4.31$. The Model-K [26] demonstrates a very good agreement with the experimental data for turbulent methane Bunsen flames over a wide range of turbulence and pressures in the range of 1 and 20 bar, the conditions typical for industrial gas turbines, spark ignition engines, etc. A Kolmogorov-Petrovski-Piskunov (KPP) analysis demonstrated analytically that at high turbulence, D needs to go to 8/3 in this model to yield the experimentally observed pressure behaviour of the turbulent flame speed s_{T} for methane flames [45]. In addition, the time-averaged value of s_{T} predicted by the model are very robust to changes in LES grid resolution [26]. The model was derived with unity Le number assumption. In the present examination, Model-K will be also used for propane fuel which has Le >1.

2.3 Brief description of Model-Z

Zimont and Lipatnikov [35] utilized the expression for Σ_{gen} as function of u'_{Δ} and the Damköhler number Da

$$\varXi = \left[1 + C_{\mathrm{Z}} \left(\frac{u'_{\Delta}}{s_{\mathrm{L}}}\right)^{3/4} \left(\frac{\Delta}{l_F}\right)^{1/4}\right], \tag{16}$$

where $C_{\mathrm{Z}} = 0.51$ is a model constant. The model was at first developed for RANS simulations and for high turbulence cases. For more details regarding the models and their derivations, the reader is referred to the original papers where these models have been presented. The models utilized in the present investigations are summarized in Table 1.

3 Experimental data considered for validation

The numerical results of the current study are validated with an extensive experimental dataset presented by Kobayashi et al. [9,12,36]. In the experimental work, the influence of pressure on cone shaped turbulent

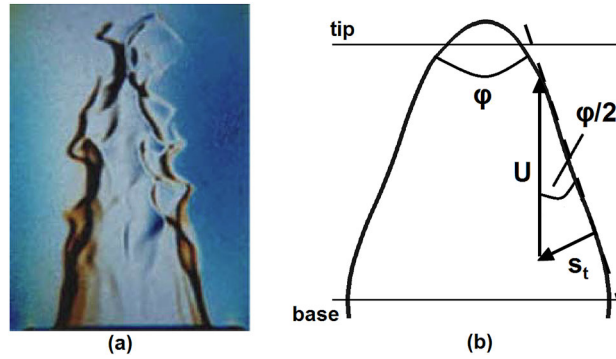**Fig. 1 a** Instantaneous Schlieren image of a typical lean premixed turbulent flame from Kobayashi et al. [36] **b** method used in the experiment to determine turbulent flame speed

premixed Bunsen flames issuing from a 20 mm diameter tube was examined in a high-pressure chamber (width 498 mm and length 600 mm). Four different types of perforated plates, installed 40 mm upstream of the chamber, were utilized as turbulence generators to create different turbulence levels and length scales. The temperature hot-wire anemometry technique was utilized to measure velocity and turbulence intensity at the centre of the burner exit. Data from lean methane/air mixtures at 1, 5, 10, 20 and 30 bar and propane/air mixtures at 1 and 5 bar at an equivalence ratio $\Phi = 0.9$ and ethylene/air mixtures at $\Phi = 0.5$, 0.7 and 0.9 for 1, 5 and 10 bar were investigated. The nozzle exit velocity U varied between 0.86 and 8.86 m/s, the maximum Reynolds number Re (based on burner exit diameter), the turbulence rms velocity u' and the transverse integral length scale l took values up to 115,000, 2.06 m/s and 1.9 mm, respectively. Flames were visualised utilizing instantaneous Schlieren photos and rapid laser tomography. A typical Schlieren picture of an instantaneous turbulent flame is shown in Fig. 1a. The averaged flame front in the experiments, defined as $\bar{c} = 0.5$ iso-contour, was obtained utilizing 50 instantaneous pictures of each flame and assuming rotational symmetry. The turbulent flame speed was then evaluated from

$$s_{\mathrm{T}} = U sin(\varphi/2), \tag{17}$$

where φ is the flame angle. It is reported that the averaged flame front exhibits a constant slope apart from the regions close to the flame tip and base. The experimental method used to calculate the turbulent flame speed is illustrated in Fig. 1b. The same method is used in the current study to evaluate the turbulent flame speed from the averaged LES $\bar{c}$-field. Figure 2 shows the experimentally observed flames in the Borghi-Peters diagram. It can be seen that the majority of the cases fall within the corrugated and wrinkled flamelet regime while few high-pressure cases fall within the thin reaction zone regime. The inlet and operating conditions of the validation cases are summarised in Table 3.

4 Numerical setup

The combustion models used in the present study are implemented in OpenFOAM. The cylindrical computational domain of diameter of 80 mm and length 120 mm is discretised using a structured mesh, refined in the flame region, hence avoiding any issue related to anisotropic, inhomogeneous grids and to limit numerical diffusion. Typical filter sizes Δ in the flame region are 0.4 mm and 0.2 mm for coarse and fine meshes, respectively. The mesh resolution is decreased (increases the cell size) in the region away from the flame region with a ratio of 1.8. The computational domain is chosen large enough so that the results are not influenced by boundaries. The convective Courant–Friedrichs–Lewy (CFL) number is set to 0.3. A first order backward Euler scheme is utilized for time discretisation. The time-steps were used in the range of 1e−6 to 4e−6 for time integration. The convective term of the momentum equation is discretized utilizing an unlimited second order linear scheme while a Total Variable Diminishing (TVD) scheme with a flux limiter (limitedLinear) is utilized to discretize the convective term in the scalar transport equation. A second order linear scheme is utilized to discretize the diffusive terms. Dirichlet boundary conditions are utilized at the inlet for all parameters, with the exception of the pressure where Neumann boundary condition (zero gradient) is used. The experimentally measured turbulence intensity and integral length scale are specified at the inlet using the turbulence generator
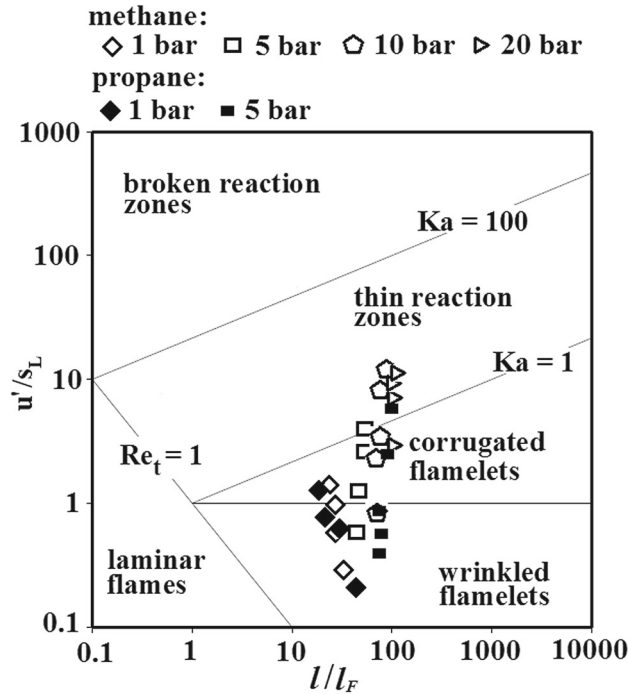
Fig. 2 Borghi-Peters diagram of the experimental data for methane and propane flames

Table 3 Characteristics of the experimental cases used for the validation of the numerical predictions made in the current study

Case	Fuel	Φ	p (bar)	U (m/s)	$u^{'}$ (m/s)	l (mm)	$u^{'}/s_{\mathrm{L}}^{0}$
1	CH_4	0.9	1	2.02	0.10	1.80	0.29
2	CH_4	0.9	1	2.33	0.20	1.43	0.59
3	CH_4	0.9	1	2.42	0.33	1.40	0.97
4	CH_4	0.9	1	2.36	0.46	1.25	1.35
5	CH_4	0.9	5	2.05	0.09	0.83	0.59
6	CH_4	0.9	5	2.53	0.19	0.99	1.25
7	CH_4	0.9	5	2.21	0.40	1.15	2.63
8	CH_4	0.9	5	3.38	0.61	1.15	4.01
9	CH_4	0.9	10	3.40	0.26	1.05	2.41
10	CH_4	0.9	10	2.11	0.36	1.10	3.33
11	CH_4	0.9	10	3.57	0.85	1.20	7.87
12	CH_4	0.9	10	4.64	1.20	1.40	11.11
13	C_3H_8	0.9	1	2.25	0.18	1.50	0.43
14	C_3H_8	0.9	1	1.50	0.26	1.25	0.61
15	C_3H_8	0.9	1	1.75	0.35	1.00	0.83
16	C_3H_8	0.9	1	2.25	0.51	0.90	1.21
17	C_3H_8	0.9	1	2.50	0.58	0.90	1.37
18	C_3H_8	0.9	5	1.55	0.04	1.15	0.17
19	C_3H_8	0.9	5	1.20	0.08	1.07	0.34
20	C_3H_8	0.9	5	2.76	0.20	0.96	0.86
21	C_3H_8	0.9	5	2.62	0.42	1.10	1.81
22	C_3H_8	0.9	5	3.51	0.63	1.20	2.72
23	C_3H_8	0.9	5	5.28	0.90	1.20	3.88

proposed by Kempf et al. [46] and implemented by Tangermann et al. [47] in OpenFOAM. In the current study, the combination of the "Total Pressure" boundary condition for pressure and "Pressure Inlet Outlet Velocity" for velocity is used at the exit to allow the backflow at the ambient conditions. This combination of boundary conditions is commonly used where inflow may take place into the domain, but the inflow velocity is not known [48]. For other variables, a mixed boundary condition is used at the exit. It switches between Neumann boundary condition (zero gradient) for flow out of the domain and Dirichlet boundary condition (fixed value)

Table 4 Summary of the grid characteristics used in the current study

Mesh	Δ (mm)	Grid size (Number of nodes)	$\left.\frac{\Delta}{l_F}\right\|_{1bar}$	$\left.\frac{\Delta}{l_F}\right\|_{10bar}$
A	0.4	0.63×10^6	8.8	27.8
C	0.2	3.99×10^6	4.4	13.9

for flow into the domain [48]. For the inflow $T = 300$ K, $k_{sgs} = 1e-5$ m^2/s^2 and $b = 1 - c = 0$ are used at the exit.

Following the experimental method used to calculate the turbulent flame speed, the filtered reaction progress variable $\bar{c}$ contours are used to estimate the turbulent flame speeds from the numerical results. The $\bar{c}$ contours are determined from time and circumferentially-averaged $\tilde{c}$ contours, using the Bray Moss Libby relation [49]

$$\bar{c} = \frac{(1 + \tau)\,\tilde{c}}{1 + \tau\tilde{c}}, \tag{18}$$

where $\tau = \rho_u/\rho_b - 1$ represents a temperature rise parameter. A least squares fit method is used to get the slope of the isoline $\bar{c} = 0.5$ (which is the correct quantity to be compared to the experimental data), neglecting the curved portion of the flame front at the flame tip and base, assessing just the linear segment of the flame. It is found that ignoring around 10% of the flame front at the flame tip and base gives a linear portion of the flame for the cases investigated in the present work. With this slope, the calculation of flame angle φ is made. The flow velocity U is known, so the flame speed can be evaluated using Eq. (17).

5 LES quality assessment

A detailed assessment of the quality of the present LES grids was done on three methodically refined grids in previous work [26]. The key features and findings of the study are described here for completeness. Table 4 demonstrates the key attributes of the grids, where Δ represents the averaged filter size in flame area. The proportion of the resolved turbulent kinetic energy k_{res} to the total turbulent kinetic energy $k_{tot} = k_{sgs} + k_{res}$ was found in the range of 85–90% and 90–95% with mesh resolutions A and C, respectively. In spite of the fact that the LES on the fine mesh resolves the turbulent kinetic energy sensibly well, a large fraction of the flame wrinkling is unresolved at high-pressures causing the subgrid combustion model to be very important at high-pressures [26]. For 10 bar case, the resolved flame wrinkling is about 20% and 12% on the fine and coarse mesh, respectively. For 5 bar case, it is about 37% and 20% on the fine and coarse mesh, respectively. On the contrary for 1 bar case, about 83% and 63% of the flame wrinkling is resolved on the fine and coarse mesh, respectively [26]. In addition, the time-averaged turbulent flame speeds predicted by the subgrid combustion model were also compared with the experimental data using three different mesh sizes in [26]. It is found that the results regarding the time-averaged $\bar{c}$ field and the derived turbulent flame speed are quite robust with respect to changes in mesh resolution. In the present work, grids with resolution A ($\Delta = 0.4$ mm) and C ($\Delta = 0.2$ mm) are utilized.

6 Results and discussion

In this section, the performance of the original and adapted versions of Model-K for non-unity Le number fuel and the performance of the original and adapted versions of Model-F under high-pressure conditions and non-unity Le number fuel will be discussed. Finally, the performance of the original and adapted versions of Model-A and Model-Z under high-pressure conditions will also be analysed.

6.1 Model-K with the Lewis number correction

Keppeler et al. [26] developed Model-K with unity Le number assumption. The model showed a very good agreement with the methane Kobayashi experimental data over a wide range of turbulence and pressure conditions in the range of 1–20 bar [26]. Thus, in the current work Model-K is adapted only for Le number
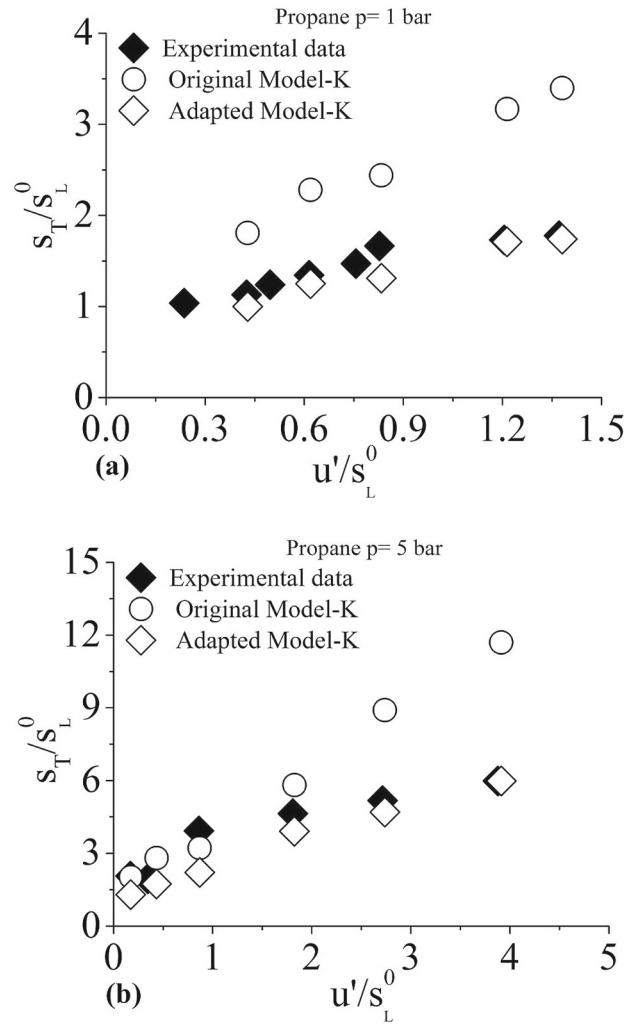
Fig. 3 Comparison of normalised turbulent flame speed s_T/s_L^0 values evaluated with the original and adapted Model-K on mesh A with experimental data for propane fuel at **a** 1 bar and **b** 5 bar

variation. The performance of the adapted Model-K with explicit incorporation of a term representing fuel effects is investigated in this section. Despite the very good agreement of Model-K results with the experimental data for methane flames (Le = 1) under atmospheric and elevated pressure conditions, when using propane fuel (Le = 1.62) it was observed that the turbulent flame speed values overestimate the experimental findings, particularly at high turbulence intensity [26]. Following the discussion in Sect. 1, the modification given by Eq. (1) was incorporated in the FSD expression of the Model-K. Apart from that all the other expressions and constants are kept same in the adapted model. The performance of the tuned and original versions of the model is investigated and compared to the experimental data of turbulent flame speeds for propane fuel at 1 and 5 bar. The normalised flame speeds s_T/s_L^0 are plotted versus u'/s_L^0 in Fig. 3a, b at 1 and 5 bar, respectively. The Model-K without Le number correction shows deviations with increasing turbulence level and the turbulent flame speed is increasingly over-predicted. However, the model scales well with the pressure. With the adapted Model-K, the predicted propane turbulent flame speed values match the experimental data very well at 1 and 5 bar, (Fig. 3). Thus Eq. (18) is proven to be a suitable way of incorporating explicit fuel effects in the Model-K. The explicit Le number term is likewise incorporated into the Model-F and the results are presented and discussed in the next section.

6.2 Investigation of the Model-F with the pressure and Lewis number corrections

Model-F is extensively used by different researchers in the open literature. Therefore, the performance of this model is investigated for both high-pressure conditions and non-unity Le numbers. In this section, the Model-F is examined by performing LES simulations with the original and adapted parameters. Earlier investigations [50–54] showed the Fureby model to be a promising representative of algebraic FSD closure technique. But it is worth noting that the most of these investigations focused a high Karlovitz number Ka cases and atmospheric methane flames. Thus, the functionality of the model at high-pressures and low Ka numbers needs to be checked. In the work by Chakraborty and Klein [50], a new power law based FSD model was proposed. The performance of the new model was compared with DNS data and thirteen other existing algebraic FSD models including the Fureby model [34]. At high Ka number cases, Model-F gives satisfactory agreement while for low Ka number cases the model under-predicts the FSD values as compared to the DNS results [50, pp. 8-11]. The authors discussed that the difference may be caused by inaccurate estimation of inner cut-off scale ε_i, the fractal dimension D and the efficiency function Γ values at these conditions. In the paper presenting the Fureby model [34], it was reported that Eq. (14c) was the only available empirical expression for D at that time. Moreover, a parameterization constant A is used to calculate ε_i. It is reported that the adopted parameterization is probably not optimal and is likely to be improved and optimized when the performance of the model is evaluated with suitable DNS and experimental data. Another problem in the Model-F is that at zero/weak subgrid turbulence level, the model wrinkling factor $\varXi = (\varepsilon_o/\varepsilon_i)^{D-2}$ approaches zero. For high turbulence cases $\varXi \gg 1$ anyway, but in the case of completely resolved flame wrinkling the wrinkling factor needs to go to one. Consequently, the original Fureby model can clearly be accurate only for cases with strong subgrid flame wrinkling. Ma et al. [51] analysed different algebraic FSD models, including Model-F, by performing LES of the ORACLES burner and Volvo Rig. In [51], Eq. (14d) of the Fureby model was used in the form $\varXi = (1 + \varepsilon_o/\varepsilon_i)^{D-2}$ so that the wrinkling factor goes to 1 in case of completely resolved flame wrinkling. It is reported that the Fureby model gives wrinkling factor values close to one in this study. The studies of [52–54] showed similar findings. The present LES study (Fig. 4) likewise demonstrates that at ambient pressure, the Model-F predicts $\varXi$ near one for low Ka number cases. In the present work, the stretched laminar flame speed s_L is utilized in the numerical simulations performed with the Model-F as in the original model proposed by Fureby [34]. Most other researchers have utilized the un-stretched laminar flame speed s_L^0, rather than stretched laminar flame speed s_L. The impact of strain effects on the performance of the original Model-F is investigated by performing LES simulations for the 10 bar cases with and without strain effects on mesh A. The normalised turbulent flame speed results are shown in Table 5. It can be seen that the turbulent flame speed is changed slightly by utilization of un-stretched laminar flame speed s_L^0, but the calculated s_T values are still under-predicted as compared to the experiment data. Thus, the Model-F does not under-predict s_T due to incorporation of strain effects on s_L.

The pressure dependence of the s_T expression of the Model-F is compared to the experimental ones for methane and propane flames using a straightforward theoretical investigation used by Muppala et al. [20] to develop a correct pressure dependence of the reaction rate closure in their combustion model. The pressure dependence of the wrinkling factor expression (Eq. (14d)) with the original and adapted parameters is determined by utilizing the pressure scaling of s_L^0, l_F and α for methane and propane fuels. The pressure dependence of the turbulent flame speed s_T is determined by $\varXi * s_L^0$. The key discoveries are summarised in Table 6. It can be seen that the model does not reproduce the experimentally observed dependence of $s_T \propto p^{0.07}$ for methane and $s_T \propto p^{0.24}$ for propane [12]. This is in agreement with the numerical results shown in Fig. 4, where a large gap is observed between the numerically predicted and experimental values obtained with original Model-F and the difference becomes larger with pressure rise. Thus, both numerical and analytical investigations argue for an adaption in the pressure dependency of s_T expression of Model-F. This is achieved by using a modified estimation of D and ε_i. In Model-F, D (Eq. 14c) achieves a limiting upper value of 2.35 and results in a negative power exponent of s_T as reported in Table 6. However, if D reaches to a constant upper value of 8/3 as used in Model-K, the constant experimentally observed pressure scaling for s_T is achieved as shown in Table 6.

The model constant A in Eq. (10) also needs to be changed from 0.75 to 9.5. The readers are referred to [55] for a detailed discussion on the tuning of model constant A. In [55, pp. 104-105], a parametric investigation of wrinkling factor $\varXi$ expressions of Model-F and Model-K (Eq. (14d) and Eq. (15e)) was done for a system that is representative of the current LES setup. It was shown that the original version of Model-F increasingly under-predicts the wrinkling factor values with increasing turbulence level as compared to the wrinkling factor values obtained with Model-K at 1 bar. The model constant A was tuned to get the right agreement between
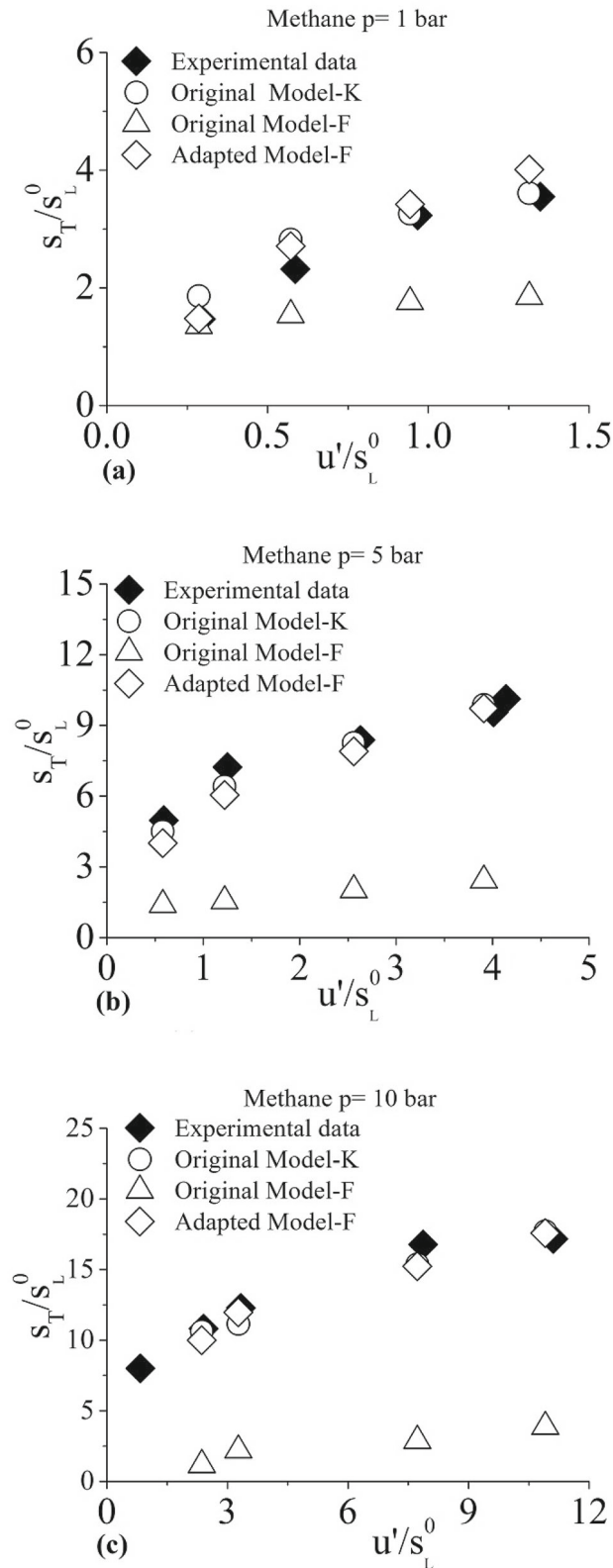
Fig. 4 Comparison of normalised turbulent flame speed s_T/s_L^0 values evaluated with the original and adapted Model-F on mesh A with experimental data and original Model-K for methane fuel at **a** 1 bar, **b** 5 bar and **c** 10 bar

Table 5 The comparison of normalised turbulent flame speed s_T/s_L^0 values predicted by the original Model-F with and without strain effects on mesh A

Case	Experimental	Original Model-F with strain effects	Original Model-F without strain effect
	s_T/s_L^0	s_T/s_L^0	s_T/s_L^0
9	10.83	1.17	1.38
12	17.13	3.87	4.03

Table 6 Comparison of pressure exponent x for different variables $f \sim p^{\wedge}x$ for the original and adapted Model-F

Original Model-F		CH$_4$	C$_3$H$_8$	Adapted Model-F	CH$_4$	C$_3$H$_8$
s_L^0		-0.50	-0.26	s_L^0	-0.50	-0.26
$\Xi\ (= s_T/s_L^0)$ with $D_{max} = 2.35$		0.29	0.26	$\Xi\ (= s_T/s_L^0)$ with $D_{max} = 8/3$	0.55	0.50
$s_L^0\,\Xi\ (= s_T)$ (Calculated)		-0.21	0	$s_L^0\,\Xi\ (= s_T)$ (Calculated)	0.05	0.24
s_T (Exp. [12])		0.07	0.24	s_T (Exp. [12])	0.07	0.24

wrinkling factor values obtained with Model-K and Model-F. The model constant $A = 9.5$ gave the correct agreement.

The inner cut-off scale can get smaller than the laminar flame thickness in the original Model-F, in contrast to findings of Driscoll [56], which states that the smallest wrinkling scale is always bigger than $C * l_F$ where C is a constant of the order of unity. In addition, the work of Kobayashi et al. [57] indicates that ε_i/l_F approaches a constant value for high-pressure turbulent flames. Therefore, ε_i is restricted to a value corresponding to l_F. The adapted Model-F is also examined on mesh A with value of $D_{max} = 2.667$ instead of $D_{max} = 2.35$ in Eq. (14c)

$$D = \frac{2.05 s_L}{u_\Delta' + s_L} + \frac{2.667 u_\Delta'}{u_\Delta' + s_L}. \tag{19}$$

The normalised turbulent flame speed values for cases 2, 4, 9 and 12 are compared to the experimental data and shown in Table 7. The adapted Model-F with Eq. (19) for D still under-predicts s_T, while the model with Eq. (15c) for D gives turbulent flame speed values and pressure scaling in agreement with the experimental data. So, Eq. (15c) is utilized in the adapted Model-F in the rest of the calculations. The modifications made to the Model-F are outlined in Table 1. For a clear picture for the reader, the key modification made to the original version of the Model-F are summarised here:

- Eq. (15c) is used for D instead of Eq. (14c)
- Model constant $A = 9.5$ is used instead of 0.75
- Eq. (1) is used to bring the Le number dependency
- Eq. (14a) is restricted to a value corresponding to l_F
- One is added inside the parenthesis of Eq. (15e)

The impact of the filter width on the time-averaged progress variable $\langle \bar{c} \rangle$, the instantaneous Favre filtered progress variable $\tilde{c}$, FSD Σ_{gen} and $|\nabla \tilde{c}|$ for case 4 and case 12 utilizing mesh A and C (hereafter signified as case-4A, case-4C, case-12A and case-12C where case-4A means case 4 from Table 4 with mesh A) are presented in Fig. 5 for the adapted Model-F. Other cases from Table 4 show similar outcomes. Figure 5a, c show the results with mesh A for pressures of 1 and 10 bar, respectively, while the results with mesh C are shown in Fig. 4b, d for 1 and 10 bar. It can be observed that $|\nabla \tilde{c}|$ contours (indicating the resolved flame surface) are more wrinkled for the finest mesh and smoother for the coarsest mesh. The instantaneous turbulent flame fronts get thinner on the fine grid, but the time-averaged turbulent flame fronts are not affected much when the mesh resolution is increased. This demonstrates the adapted Model-F is also robust to moderate changes of grid spacing.

The LES results when using the original and adapted Model-F for methane and propane fuels are compared with the experimental data and the Model-K. For methane, Fig. 4a–c show normalized flame speeds s_T/s_L^0 plotted versus u'/s_L^0 for 1, 5 and 10 bar, respectively. In contrast to original Fureby model, the adapted Model-F now gives excellent quantitative agreement with the experimental data and yields the right pressure scaling.

Table 7 The comparison of normalised turbulent flame speed s_T/s_L^0 values predicted by the adapted Model-F utilising Eq. (19) and Eq. (15c) on mesh A

Pressure [bar]	Case	Experimental	Model-F with Eq. (19) for D	Model-F with Eq. (15c) for D
		s_T/s_L^0	s_T/s_L^0	s_T/s_L^0
1	2	2.32	1.99	2.74
	4	3.55	2.74	4.02
10	9	10.83	3.32	9.71
	12	17.13	12.22	17.59
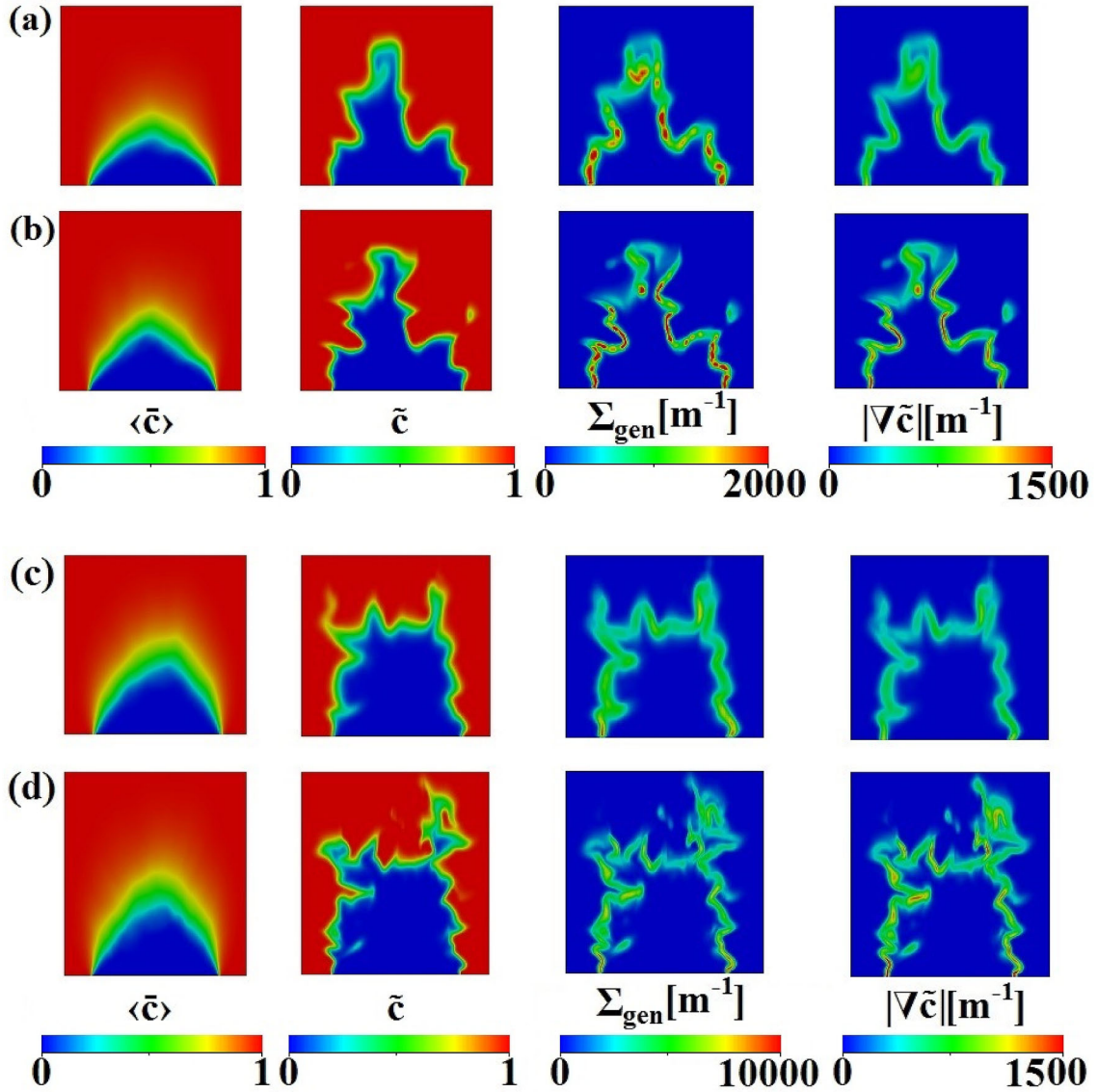
Fig. 5 Influence of filter width on the time-averaged $\langle \bar{c} \rangle$, instantaneous flame surface $\tilde{c}$, FSD Σ_{gen} and $|\nabla \tilde{c}|$ contours with the adapted Model-F for **a** case-4A, **b** case-4C, **c** case-12A and **d** case-12C
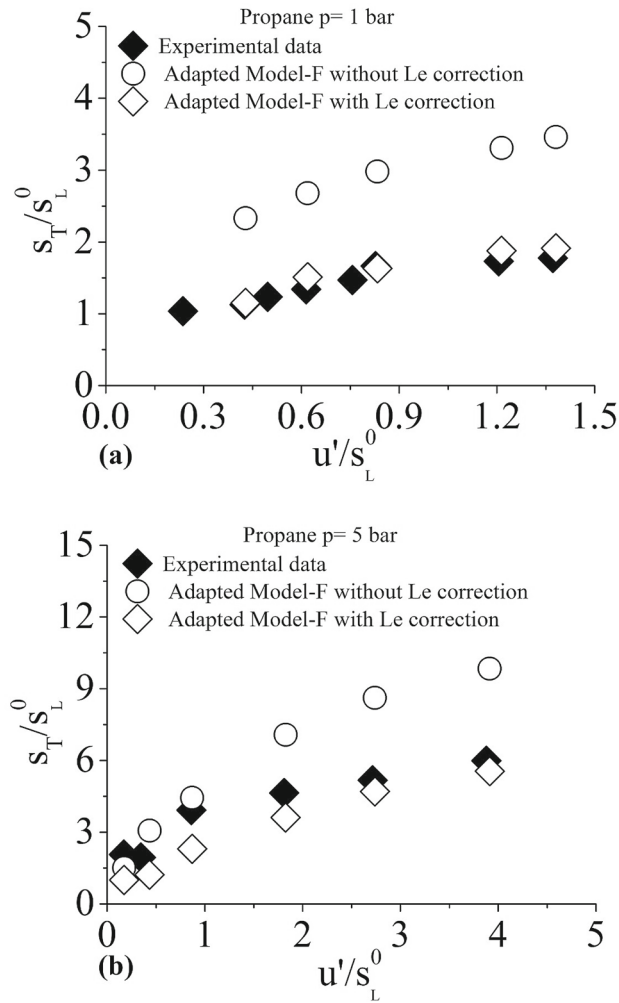
Fig. 6 Comparison of normalised turbulent flame speed s_T/s_L^0 values evaluated with the adapted Model-F on mesh A with experimental data for propane fuel at **a** 1 bar and **b** 5 bar

Figure 6a, b show similar plots for propane fuel utilizing the adapted Model-F with and without the Le number correction given by Eq. (1). The adapted Model-F with the Le number correction also shows excellent performance compared to the experimental data over a wide range of turbulence and pressures in the range of 1–5 bar.

6.3 Numerical examination of the models concerning pressure dependency

The Le number dependency in the Model-F is brought by using the expression 1/Le as used in the Model-K. The results show that the adapted Model-K and Model-F give quite a good performance for non-unity Le number fuel and a reasonable agreement with the experiments. Model-A and Model-Z are only adapted for pressure variation for the sake of brevity. The authors believe that the expression 1/Le can also be used in these models to introduce the Le number dependency. Model-A and Model-Z LES simulations are performed for methane fuel at 1, 5 and 10 bar. Figure 7 shows the instantaneous and time-averaged progress variable contours from the original Model-A and Model-Z compared to Model-K for case-4A. It can be observed that longer flames are predicted with the original Model-A and Model-Z. Table 8 gives a comparison of normalised turbulent flame speed s_T/s_L^0 values predicted by the original Model-A and Model-Z on mesh A with the experimental data and Model-K. For the 1 bar cases the turbulent flame speed values are under-predicted. The experimentally observed normalised turbulent flame speed s_T/s_L^0 for case 4 is 3.55 while s_T/s_L^0 from Model-K, Model-A and
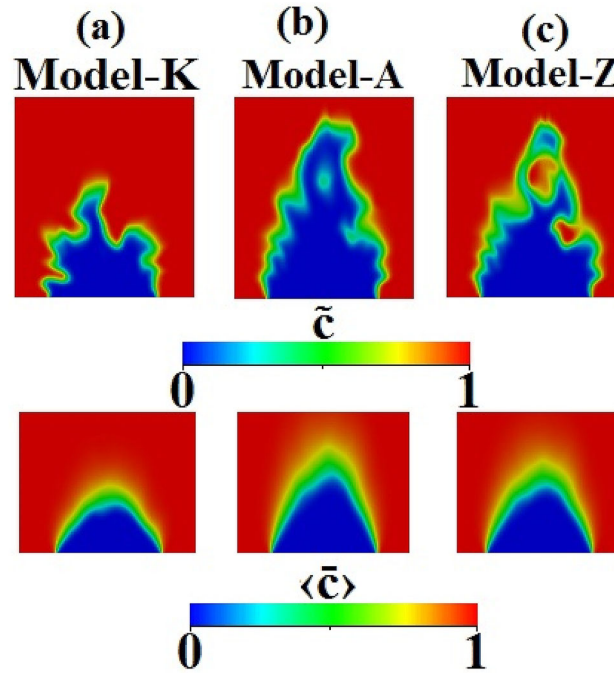
Fig. 7 Comparison of time-averaged and instantaneous progress variable contours for case-4A with original versions of **a** Model-K, **b** Model-A and **c** Model-Z

Table 8 The comparison of normalised turbulent flame speed s_T/s_L^0 values predicted by Model-A and Model-Z with and without explicit pressure correction term on mesh A with the experimental data and Model-K

Case	s_T/s_L^0					
	Experimental	Original Model-K	Original Model-A	Model-A with $(p/p_0)^n$	Original Model-Z	Model-Z with $(p/p_0)^n$
3	3.23	3.26	2.42	3.10	2.72	3.14
4	3.55	3.60	2.60	3.35	2.89	3.36
7	8.35	8.25	3.78	8.14	3.77	7.10
8	9.54	9.87	4.58	9.74	4.15	8.00
10	12.31	11.15	5.02	12.4	4.09	10.01

Model-Z are 3.60, 2.60 and 2.89, respectively. The lower flame speeds from Model-A and Model-Z suggest a tuning of model constants to reach the right quantitative agreement with the experimental data at 1, 5 and 10 bar. Good agreement for the Model-A and Model-Z could be achieved by changing the model constants and by incorporating an explicit pressure correction term $(p/p_0)^n$ where exponent n is a constant similar to Muppala et al. [20] used in their algebraic reaction rate closure model. Obviously, from a theoretical point of view an explicit empirical pressure correction term is undesirable because of the absence of physical reasoning.

The turbulent flame speeds from LES results utilizing the Model-A and Model-Z with adapted model constants and with pressure correction term are noted in Table 8. The adaptations made to the models are presented in Table 1. The models with empirical pressure scaling reflect the experimental pressure dependence and turbulent flame speed values exhibit fairly good agreement with the experimental data. The method to calculate the exponent n for Model-A and Model-Z is shown in Appendix-1.

7 Conclusion

A subgrid LES combustion model should include the effects of pressure and fuel type in the reaction rate closure to claim its generality. An extensive numerical investigation is performed in the present study to determine these two significant effects utilizing main elements of some well-known algebraic FSD models

accessible in the open literature. The numerical results are compared with experimental data for lean turbulent Bunsen flames utilizing methane and propane fuels for various flow conditions at pressures in the range of 1–10 bar. With the original versions of the selected models, the turbulent flame speed is under-predicted with discrepancy increasing for high-pressures. The model constants were tuned and suitable pressure corrections were used to achieve correct quantitative agreement and pressure dependency of the turbulent flame speed with the experimental data. A new term (1/Le) was also incorporated introducing the fuel effects in the reaction rate closure of the Model-K and Model-F. With these adaptations the models predict the turbulent flame speed values in an excellent agreement with the experimental data of the turbulent flames.

Appendix 1

This section shows the calculation of pressure exponent n of the explicit pressure correction term for adapted Model-A and Model-Z.

Model-A

For $\Xi \gg 1$, Eq. (13) for Model-A without an explicit pressure correction term can be written as:

$$\Xi = \left[C_A \Gamma \frac{u'_\Delta}{s_L^0} \right] = \frac{s_T}{s_L^0}, \tag{A1}$$

$$\Xi * s_L^0 = \left[C_A \Gamma \frac{u'_\Delta}{s_L^0} \right] s_L^0 = s_T. \tag{A2}$$

From Eq. (A2), the pressure dependence of the predicted turbulent flame speed s_T from the Model-A is calculated and compared with the experimentally observed pressure dependence of turbulent flame speed, which is $s_T \propto p^{0.07}$ for methane [29]. For methane using $s_L^0 \propto p^{-0.5}$ and $l_F \propto p^{-0.5}$, the pressure dependence of the efficiency function from Eq. (10) is found to be $\Gamma \propto p^{1/3}$. Putting the pressure dependence values of s_L^0 and Γ in Eq. (A2) and we get $\Xi * s_L^0 \propto p^{1/3}/p^{-0.5} * p^{-0.5} = p^{1/3}$. The pressure exponent of 0.33 is larger than the experimental one 0.07. Now an explicit pressure correction term $(p/p_0)^n$ is introduced in Eq. (A1) with a value of n giving the correct pressure dependence of s_T:

$$\left(\frac{p}{p_0} \right)^n * \Xi * s_L^0 = \left(\frac{p}{p_0} \right)^n \left[C_A \Gamma \frac{u'_\Delta}{s_L} \right] s_L^0. \tag{A3}$$

For Model-A, n is found to be -0.25 which is giving the experimental dependence of s_T close to zero for methane i.e. $(p/p_0)^n * \Xi * s_L^0 \propto p^{-0.25} * p^{1/3}/p^{-0.5} * p^{-0.5} = p^{0.08}$. It is noted that in above calculations u'_Δ is taken to be independent of pressure. At high Reynolds number and constant inlet velocity, u' will be approximately constant. However, with increasing pressure and thus increasing Reynolds number the Kolmogorov length decreases. At constant filter width the total subgrid turbulent energy and therefore u'_Δ may increase slightly. However, as discussed in Sect. 6.3, LES simulation using the adapted Model-A with $n = -0.25$ gives very good agreement of the predicted turbulent flame speed with the experimental data, justifying the assumption of a small effect of a pressure variation of u'_Δ on the turbulent flame speed.

Model-Z

A similar analysis is performed for the Model-Z with Eq. (16) and n is found to be 0.15.

References

1. Peters, N.: Turbulent Combustion. Cambridge University Press, Cambridge (2000)
2. Menon, S., Jou, W.: Large Eddy simulations of combustion instability in an axisymmetric ramjet combustor. Combust. Sci. Technol. **75**(1–3), 53–72 (1991)

3. Butler, T.D., O'Rourke, P.J.: A numerical method for two dimensional unsteady reacting flows. Proc. Symp. (Int.) Combust. **16**(1), 1503–1515 (1977)
4. Colin, O., Ducros, F., Veynante, D., Poinsot, T.: A thickened flame model for Large Eddy simulations of turbulent premixed combustion. Phys. Fluids **12**(7), 1843–1863 (2000)
5. Boger, M., Veynante, D., Boughanem, H., Trouvé, A.: Direct numerical simulation analysis of flame surface density concept for Large Eddy simulation of turbulent premixed combustion. Proc. Symp. (Int.) Combust. **27**(1), 917–925 (1998)
6. Hawkes, E., Cant, R.S.: A flame surface density approach to Large Eddy simulation of premixed turbulent combustion. Proc. Combust. Inst. **28**(1), 51–58 (2000)
7. Duwig, C., Fureby, C.: Large Eddy simulation of unsteady lean stratified premixed combustion. Combust. Flame **151**(1–2), 85–103 (2007)
8. Aluri, N., Muppala, S.P.R., Dinkelacker, F.: Large Eddy simulation of lean premixed turbulent flames of three different combustion configurations using a novel reaction closure. Flow Turbul. Combust. **80**(2), 207–224 (2008)
9. Kobayashi, H., Nakashima, T., Tamura, T., Maruta, K., Niioka, T.: Turbulence measurements and observations of turbulent premixed flames at elevated pressures up to 3.0 MPa. Combust. Flame **108**(1–2), 104–117 (1997)
10. Bounif, A., Aris, A., Gökalp, I.: Pressure effects on the spectral behaviour of the thermal field in non-reacting and Low Damköhler reacting flows. Int. J. Therm. Sci. **38**(9), 819–831 (1999)
11. Soika, A., Dinkelacker, F., Leipertz, A.: Pressure influence on the flame front curvature of turbulent premixed flames: comparison between experiment and theory. Combust. Flame **132**(3), 451–462 (2003)
12. Kobayashi, H., Kawabata, Y., Maruta, K.: Experimental study on general correlation of turbulent burning velocity at high pressure. Proc. Symp. (Int.) Combust. **27**(1), 941–948 (1998)
13. Poinsot, T., Veynante, D.: Theoretical and Numerical Combustion, 2nd edn. Edwards, Morningside (2005)
14. Rasool, R., Chakraborty, N., Klein, M.: Algebraic flame surface density modelling of high pressure turbulent premixed Bunsen flames. Flow Turbul. Combust. (2020)
15. Alqallaf, A., Klein, M., Dopazo, C., Chakraborty, N.: Evolution of flame curvature in turbulent premixed Bunsen flames at different pressure levels. Flow Turbul. Combust. **103**, 439–463 (2019)
16. Wnag, X., Jin, T., Xie, Y., Kuo, K.L.: Pressure effects on flame structures and chemical pathways for lean premixed turbulent H_2/air flames: Three-dimensional DNS studies. Fuel **215**, 320–329 (2018)
17. Wang, Z., Magi, V., Abraham, J.: Turbulent flame speed dependencies in lean methane-air mixtures under engine relevant conditions. Combust. Flame **180**, 53–62 (2017)
18. Savard, B., Lapointe, S., Teodorczyk, A.: Numerical investigation of the effect of pressure on heat release rate in iso-octane premixed turbulent flames under conditions relevant to SI engines. Proc. Combust. Inst. **36**, 3543–3549 (2017)
19. Devaud, C., Bushe, W.K., Bellan, J.: Assessment of Conditional Source-Term Estimation for High Pressure turbulent combustion modelling. AIAA SciTech Forum, San Diego, California (2019)
20. Muppala, S.P.R., Aluri, N.K., Dinkelacker, F., Leipertz, A.: Development of an algebraic reaction rate closure for the numerical calculation of turbulent premixed methane, ethylene and propane/air flames for pressures up to 1.0 MPa. Combust. Flame **140**(4), 257–266 (2005)
21. Aluri, N.K., Muppala, S.P.R., Dinkelacker, F.: A test of validation of turbulent premixed models for high-pressure Bunsen flames. In: Proceedings European Combust Meeting (2005)
22. Aluri, N.K., Muppala, S.P.R., Dinkelacker, F.: Substantiating a fractal-based algebraic reaction closure of premixed turbulent combustion for high pressure and the Lewis number effects. Combust. Flame **145**, 663–774 (2006)
23. Dinkelacker, F., Manickam, B., Muppala, S.P.R., Aluri, N.K.: Modelling and simulation of lean premixed turbulent methane/hydrogen/air flames for two flow configurations. In: Proceedings of CHT-08 ICHMT International Symposium on Advances in Computational Heat Transfer (2008)
24. Dinkelacker, F., Manickam, B., Muppala, S.P.R.: Modelling and simulation of lean premixed turbulent methane/hydrogen/air flames with an effective Lewis number approach. Combust. Flame **158**(9), 1742–1749 (2011)
25. Lindstedt, R., Váos, E.: Modelling of premixed turbulent flames with second moment methods. Combust. Flame **116**(4), 461–485 (1999)
26. Keppeler, K., Tangermann, E., Allauddin, U., Pfitzner, M.: LES of low to high turbulent combustion in an elevated pressure environment. Flow Turbul. Combust. **92**(3), 767–802 (2014)
27. Allauddin, U., Keppeler, K., Pfitzner, M.: Turbulent premixed les combustion models based on fractal flame surface density concepts. In: Proceedings of ASME Turbo Expo: Turbine Technical Conference and Exposition GT2014 June 16–20, 2014. German, Düsseldorf (2014)
28. Allauddin, U., Pfitzner, M.: Development of a RANS premixed turbulent combustion model based on the algebraic flame surface density concept. J. Eng. Gas Turbines Power **141**, 1–8 (2019)
29. Lipatnikov, A.N., Chomiak, J.: Molecular transport effects on turbulent flame propagation and structure. Prog. Energy Combust. Sci. **31**(1), 1–73 (2005)
30. Abdel-Gayed, R.G., Bradley, D., Hamid, M.N., Lawes, M.: Lewis number effects on turbulent burning velocity. Symp. (Int.) Combust. **20**(1), 505–512 (1984)
31. Chakraborty, N., Cant, R.S.: Effects of Lewis number on flame surface density transport in turbulent premixed combustion. Combust. Flame **158**(9), 1768–1787 (2011)
32. Klein, M., Chakraborty, N., Pfitzner, M.: Analysis of the combined modelling of sub-grid transport and filtered flame propagation for premixed turbulent combustion. Flow Turbul. Combust. **96**(4), 921–938 (2016)
33. Angelberger, C., Veynante, D., Egolfopoulos, F., Poinsot, T.: Large Eddy simulations of combustion instabilities in premixed flames. In: Proceedings of Summer Program, Center for Turbulence Research, 5–31 July 1998, NASA Ames/Stanford University, pp. 61-82 (1998)
34. Fureby, C.: A fractal flame wrinkling Large Eddy simulation model for premixed turbulent combustion. Proc. Combust. Inst. **30**(1), 593–601 (2005)
35. Zimont, V., Lipatnikov, A.: A numerical model of premixed turbulent combustion of gases. Chem. Phys. Rep. **14**(7), 993–1025 (1995)

36. Kobayashi, H., Tamura, T., Maruta, K., Niioka, T., Williams, F.A.: Burning velocity of turbulent premixed flames in a high pressure environment. Proc. Combust. Inst. **26**(1), 389–396 (1996)
37. Gouldin, F.: An application of fractals to modelling premixed turbulent flames. Combust. Flame **68**(3), 249–266 (1987)
38. Allauddin, U., Klein, M., Pfitzner, M., Chakraborty, N.: A-priori and a-posteriori analysis of algebraic flame surface density modelling in the context of Large Eddy Simulation of Turbulent Premixed Combustion. Numer. Heat Transfer Part A **71**(2), 153–171 (2014)
39. Schumann, U.: Subgrid Scale Model for Finite Difference Simulations of Turbulent Flows in Plane Channels and Annuli. J. Comput. Phys. **18**(1), 376–404 (1975)
40. Fureby, C., Tabor, G., Weller, H.G., Gosman, A.D.: A comparative study of subgrid scale models in homogeneous isotropic turbulence. Phys. Fluids **9**(5), 1416–1429 (1997)
41. Clavin, P.: Dynamic behaviour of premixed flame fronts in laminar and turbulent flows. Prog. Energy Combust. **11**(1), 1–59 (1985)
42. Muller, U.C., Bollig, M., Peters, N.: Approximations for burning velocities and Markstein numbers for lean hydrocarbon and methanol flames. Combust. Flame **108**(3), 349–356 (1997)
43. Hawkes, E., Cant, R.S.: Implications of a flame surface density approach to Large Eddy simulation of turbulent premixed combustion. Combust. Flame **126**(3), 1617–1629 (2001)
44. Meneveau, C., Poinsot, T.: Stretching and quenching of flamelets in premixed turbulent combustion. Combust. Flame **86**(4), 311–332 (1999)
45. Keppeler, R.: Entwicklung und Evaluierung von Verbrennungsmodellen für die Large Eddy Simulation der Hochdruck-Vermischverbrennung. PhD. Thesis, University of Bundeswehr, Munich (2013)
46. Kempf, A., Klein, M., Janicka, J.: Efficient generation of initial and inflow conditions for transient turbulent flows in arbitrary geometries. Flow Turbul. Combust. **74**(1), 67–84 (2005)
47. Tangermann, E., Pfitzner, M.: Evaluation of combustion models for combustion-induced vortex break-down. J. Turbul. **10**, N7 (2009)
48. OpenFOAM CFD Limited. OpenFOAM User Guide http://cfd.direct/openfoam/user-guide/ (Access on 07 May 2020)
49. Bray, K.N.C., Moss, J.B.: A unified statistical model of the premixed turbulent flame. Acta Astronaut. **4**(3–4), 291–319 (1977)
50. Chakraborty, N., Klein, M.: A priori direct numerical simulation assessment of algebraic flame surface density models for turbulent premixed flames in the context of Large Eddy simulation. Phys. Fluids **20**(8), 85–108 (2008)
51. Ma, T., Stein, O.T., Chakraborty, N., Kempf, A.M.: A posteriori testing of algebraic flame surface density models for LES. Combust. Theor. Model. **17**(3), 431–482 (2013)
52. Ma, T., Stein, O.T., Chakraborty, N., Kempf, A.M.: A posteriori testing of the flame surface density transport equation for LES. Combust. Theor. Model. **18**(1), 32–64 (2014)
53. Katragadda, M., Chakraborty, N., Cant, R.S.: A priori assessment of algebraic flame surface density models in the context of Large Eddy simulation for non-unity Lewis number flames in the thin reaction zones regime. J. Combust. 2012, article ID 794671, 17 pages (2012)
54. Katragadda, M., Chakraborty, N., Cant, R. S.: Effects of turbulent reynolds number on the performance of algebraic flame surface density models for Large Eddy simulation in the thin reaction zones regime: a direct numerical simulation analysis. J. Combust. 2012, article ID 353257, 13 pages (2012)
55. Allauddin, U.: Modelling of Turbulent Premixed Flames using LES and RANS Methods. PhD Thesis, University of Bundeswehr, Munich (2017)
56. Driscoll, J.F.: Turbulent premixed combustion: flamelet structure and its effect on turbulent burning velocities. Prog. Energy Combust. Sci. **34**(1), 91–134 (2008)
57. Kobayashi, H., Kawazoe, H.: Flame instability effects on the smallest wrinkling scale and burning velocity of high-pressure turbulent premixed flames. Proc. Combust. Inst. **28**(1), 375–382 (2000)